Local raster scanning for high-speed imaging of biopolymers in atomic force microscopy

Peter I. Chang, Peng Huang, Jungyeoul Maeng, and Sean B. Andersson
Department of Mechanical Engineering, Boston University, Boston, Massachusetts 02215, USA

A novel algorithm is described and illustrated for high speed imaging of biopolymers and other string-like samples using atomic force microscopy. The method uses the measurements in real-time to steer the tip of the instrument to localize the scanning area over the sample of interest. Depending on the sample, the scan time can be reduced by an order of magnitude or more while maintaining image resolution. Images are generated by interpolating the non-raster data using a modified Kriging algorithm. The method is demonstrated using physical simulations that include actuator and cantilever dynamics, nonlinear tip-sample interactions, and measurement noise as well as through scanning experiments in which a two-axis nanopositioning stage is steered by the algorithm using simulated height data. © 2011 American Institute of Physics. [doi:10.1063/1.3600558]

I. INTRODUCTION

The atomic force microscope (AFM) (Ref. [1]) is a versatile instrument for studying systems with nanometer-scale features. Its high spatial resolution, ability to work in different environments, and flexibility to be modified to measure many different interactions make it a powerful tool. It continues to have a major impact on a variety of fields, including materials science, biology, and nanotechnology. Its application remains limited, however, by its temporal resolution, with commercial instruments often taking on the order of minutes to generate a single image. As a result, there is great interest in high speed AFM with the goal of achieving video-rate and faster imaging.[2]

High-speed AFM approaches can be broadly placed in two categories. The first is the use of alternative physical designs. For example, researchers have built small cantilevers,[3] designed microresonators with mechanical feedback,[4] utilized serially connected scanning stages,[5] and constructed scanners with high resonance frequencies.[6] The second category is to apply advanced control techniques such as combined feedforward/feedback control,[7] model-based feedforward control,[8] and iterative learning control.[9] Combinations of such approaches have yielded video rate imaging.[10,11]

In general, existing approaches to high-speed AFM seek to move the tip more rapidly through the raster-scan pattern while maintaining image quality. Our *local raster-scan* scheme takes a different approach: imaging time is reduced by *reducing the amount of sampling*. The information measured by the instrument is used in real-time to adjust the scanning process. The algorithm, designed for biopolymers and other samples that can be modeled as a planar curve, tracks the sample such that the measurements are restricted to the neighborhood of the sample. Overall scanning time is reduced not by increasing the tip speed but by decreasing the scan area. Depending on the sample, an order-of-magnitude or better reduction in imaging time can be achieved. Furthermore, the method is complementary to other high-speed

imaging methods. Combining the algorithm with such techniques can lead to further improvements in imaging time.

The resulting data are non-raster and generating an image from the set is non-trivial. We have developed a modified Kriging method[12] that produces an accurate image from the data through an interpolation scheme that takes advantage of the structure of the data. We use that approach in this work.

II. ALGORITHM

A. Local raster scanning

Local raster scanning operates as a high-level feedback loop around the AFM system, as illustrated in Fig. 1. There are four blocks in the controller loop: *detection*, *estimation*, *filtering*, and *tip trajectory design*. The algorithm actively tracks the spatial evolution of the underlying sample, scanning the tip transversely while moving along the sample.

An example trajectory of the local raster-scan algorithm is shown in Fig. 2, layered on a standard raster-scanned DNA image. The tip trajectory (sinusoidal segments) crosses back and forth over the DNA, driven by an estimation of the spatial evolution of the edge of the sample (short line segments).

The evolution of the sample path, denoted r, is modeled using the Fernet-Serret (F-S) frame equations,

$$r'(s) = q_1(s), \tag{1a}$$

$$q_1'(s) = \kappa(s)q_2(s), \tag{1b}$$

$$q_2'(s) = -\kappa(s)q_1(s), \tag{1c}$$

where prime denotes the derivative with respect to the arclength s, $\kappa(s)$ is the curvature at s, $q_1(s)$ is the tangent to r at s, and $q_2(s)$ is the normal to r at s. The vectors $q_1(s)$ and $q_2(s)$ can be expressed using a heading direction $\theta(s)$, by $q_1 = [\cos\theta(s)\sin\theta(s)]'$ and $q_2 = [-\sin\theta(s)\cos\theta(s)]'$.[13] The curve is then determined by measuring the local curvature and heading direction and then solving Eq. (1) until the next measurement.
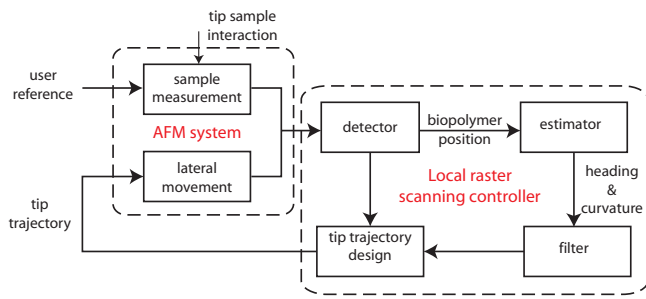
     82, 063703-1

FIG. 1. (Color online) Block diagram of the local raster-scan control loop. Driven by the data acquired by the AFM, the *detector* block determines the current position of the sample in the scan. These positions are used by the *estimator* block to determine the geometric parameters driving the spatial evolution of the path of the sample. After *filtering*, these values are fed to the *tip trajectory* block which estimates the evolution of the sample and, from that, the desired trajectory of the tip.

Given a curve $r(\cdot)$, the AFM tip trajectory is determined by

$$r_{tip}(s) = r(s) \pm A \sin(\omega s) q_2(s), \qquad (2)$$

where A is the scan amplitude and ω is the spatial frequency. Note that both A and ω are user inputs that can be chosen. This path is designed to provide a smooth trajectory for the tip to ensure accurate tracking by the low-level piezo controllers.

In order to implement the algorithm, the arclength parameter must be converted to a time parameter such that the tip trajectory is expressed as $r_{tip}(s) = r_{tip}(s(t))$. This relationship is given by fixing the speed of the tip, v_{tip} and then inverting the equation,[14]

$$t = \frac{1}{v_{tip}} \int_0^s \sqrt{(1 - A\kappa \sin(\omega\sigma))^2 + A^2\omega^2 \cos^2(\omega\sigma)} \, d\sigma.$$
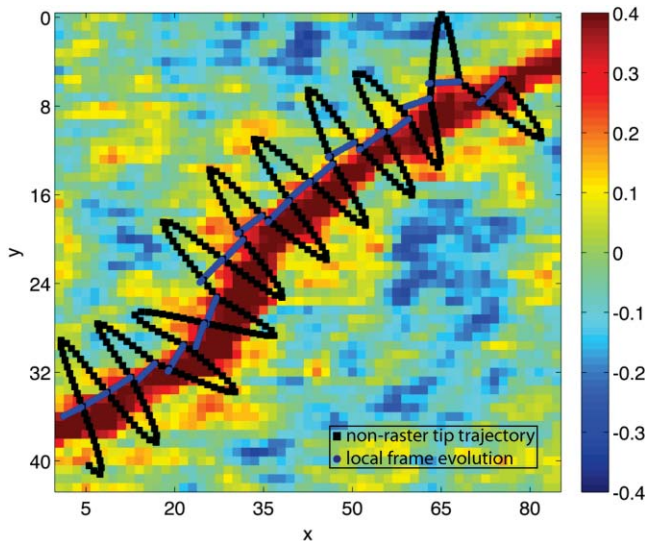
$$(3)$$

FIG. 2. (Color online) Illustration of a typical local raster scanning trajectory. The underlying image is a portion of the height data from a standard raster-scan of DNA using a commercial AFM system. The tip trajectory (sinusoidal segments) is driven by the estimation of the evolution of the edge of the DNA sample (short line segments).

In practice, the inversion of Eq. (3) is done off-line and stored either in a look-up table or approximated with a function such as a low-order polynomial.

Each step of the algorithm begins by detecting a transition of the tip between the substrate and the sample. The main function of the detector block is to determine such a transition and produce a measurement of the position of that transition, denoted r_k where k indexes crossing of the sample. Depending on the operational mode of the AFM, there are a variety of ways to perform this detection. Examples include the use of a maximum likelihood estimator based on the height measurements[15] or a transient signal observer that monitors the amplitude signal of an AFM operated in intermittent contact (tapping) mode.[16]

When the detector block determines a new transition, the index k is incremented and the new value of r_k is passed to the estimator block. This block uses past values of the crossing positions to determine the heading direction and curvature as follows. For the heading direction, the tangent vector to the sample curve at r_k is estimated using an Euler approximation to the derivative,

$$\hat{q}_{1k} = \frac{r_k - r_{k-1}}{\|r_k - r_{k-1}\|},$$

where $\| \cdot \|$ is the Euclidean norm. The estimate of the heading direction, $\hat{\theta}$, is given by the angle of $\hat{q}_{1k}$. The estimate of the curvature, $\hat{\kappa}$ is calculated from Heron's formula,

$$\hat{\kappa} = \pm 4 \frac{\sqrt{l(l-a)(l-b)(l-c)}}{abc},$$

where l is the semi-perimeter of the triangle defined by the three points r_k, r_{k-1}, and r_{k-2} and a, b, and c are the lengths of the sides of that triangle.

To mitigate the effect of noise in the estimates of $\hat{\theta}$ and $\hat{\kappa}$ (arising from noise in the estimate of r_k and amplified due to the numerical derivatives), a Kalman filter is used to filter $(\hat{\theta}, \hat{\kappa})$.[13]

The filtered values are then sent to the tip trajectory design block. Here, they are used in Eq. (1) to propagate forward an estimate of the path of the sample and then in Eq. (2) to produce the desired tip trajectory. This trajectory is then sent to the low-level controllers to achieve the tip motion.

1. Discussion of curvature assumptions

The local raster-scan algorithm assumes that the underlying sample maintains a constant curvature between crossings of the tip. Practically, this means that the curvature should change slowly with respect to the distance between those crossings. If this assumption fails, due either to the sample itself or noise in the measurements, then loss of tracking can occur (see Ref. 17 for a detailed discussion of this issue). It is therefore important to select the resolution parameter ω large enough to ensure tracking of the particular sample under study. While the actual curvatures are not known *a priori*, it is possible to establish realistic bounds on both the curvature and the rate of change of curvature using their persistence length or descriptions such as a wormlike chain model.[18] These bounds can then be used to guide the
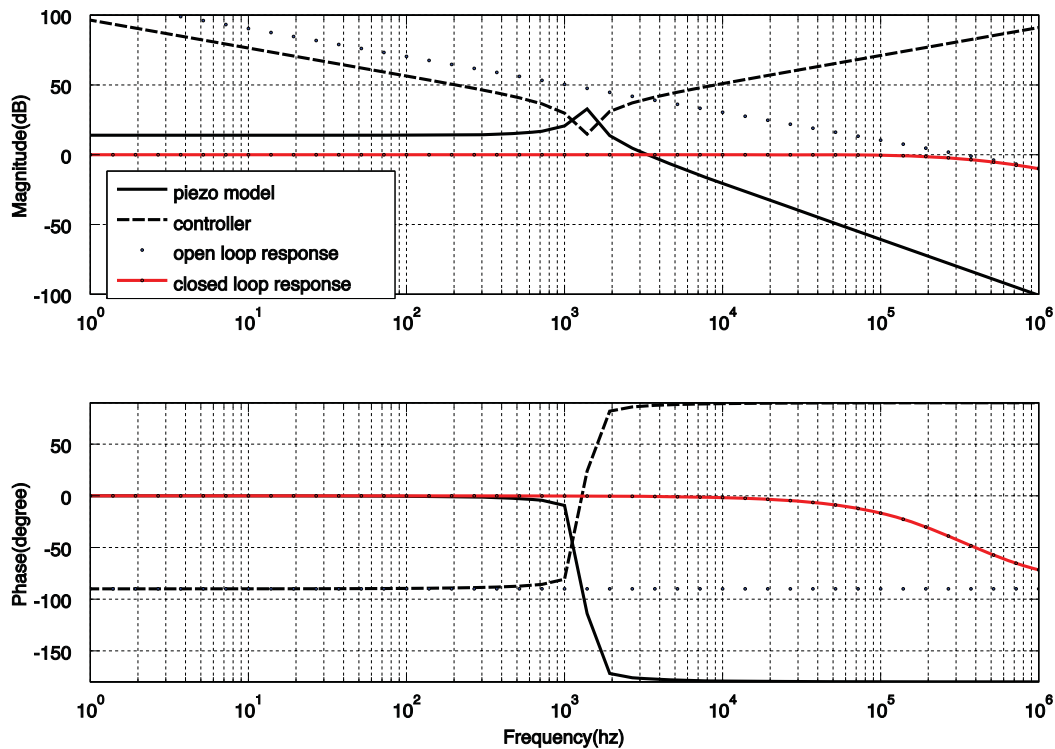
FIG. 3. (Color online) Bode plot of the piezo dynamics (solid line with resonant peak in the magnitude), the PID controller (dashed line with a notch in the magnitude), and the closed loop system (solid line with no resonant peak) used in the simulation. The closed loop bandwidth was over 50 kHz.

selection of scan parameters so as to ensure that the assumption of constant curvature holds reasonably well.

The imaging time is directly proportional to the total path length traveled by the tip. This in turn is increased by increasing the value of ω. Selecting ω sufficiently high so as to ensure tracking of the biopolymer along a region of maximum curvature will slow down the imaging process. A logical refinement of the algorithm is to allow for adaption on the value of ω based on the estimate of the curvature, increasing it where necessary to maintain tracking and relaxing it when possible to minimize imaging time.

B. Imaging from local raster scanning data

Data collected along the local raster-scan trajectory are by design not evenly spaced and thus interpolation must be used to generate an image from them. There are a variety of techniques for interpolating non-raster data for imaging, including polygonal interpolation, averaging, and the inverse distance method. We have chosen two methods for re-creating images from the local raster scanning on biopolymers, a mod-

ified Kriging interpolation[19] tailored to stringlike samples and standard Delaunay triangulation.[20]

Kriging models the sampled data as outcomes of random variables and interpolates intermediate values with an unbiased estimator that minimizes the error covariance among all linear estimations. Due to the structure of our samples, the information content in the acquired data is heavily anisotropic, with data being related primarily along the sample. The modified Kriging method takes this into account to produce accurate images[12] (cf. Figs. 5(c) and 6(c)). Because of its high computational cost, Kriging is best-suited for off-line image generation. In order to provide visual feedback for the user during scanning, one can use standard Delaunay triangulation.[12]

III. SIMULATIONS

To illustrate the effectiveness of the local raster-scan algorithm, a detailed dynamic simulator of an AFM system was developed. The simulator modeled the dynamics of the actuators, the low-level controllers, and the nonlinear tip-sample dynamics and allowed us to produce both standard raster-scan and local raster-scan images of the same sample.

A. Simulator setup

FIG. 4. Sample profile used in the simulator.

Since there are a variety of different physical designs for AFMs,[21] we used a generic model to capture the basic dynamics of the x, y, and z components of the AFM system. Each axis was modeled as the same second order system described by the Bode plot in Fig. 3. A low-level Proportional-
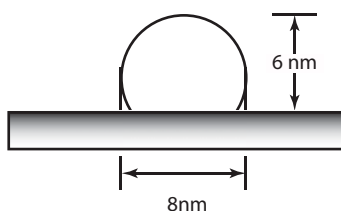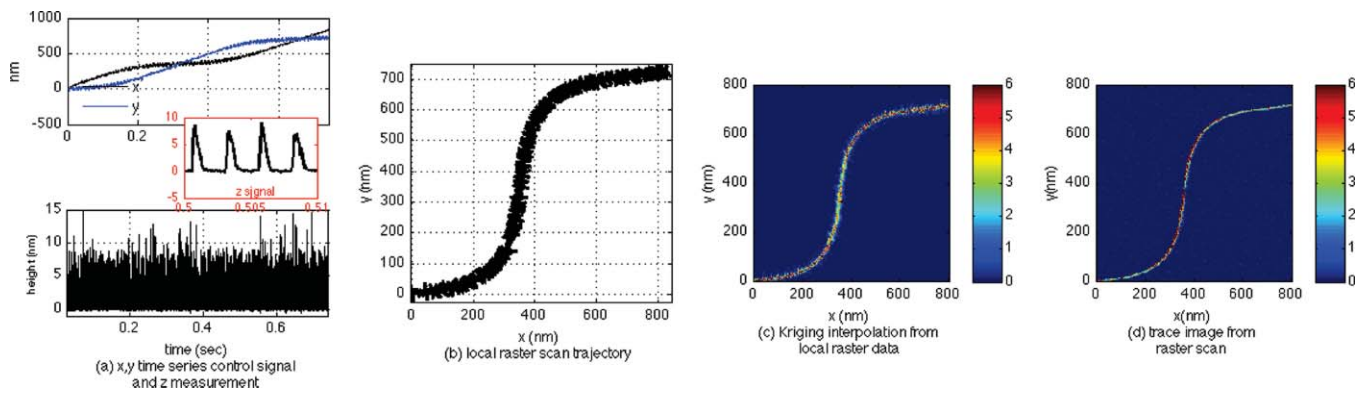
FIG. 5. (Color online) Simulation result of local raster ((a)–(c)) and raster-scan (d) on a sinusoidal test curve. Image (b) clearly indicates that the local raster-scan kept the tip in the vicinity of the sample. The tip speed in both images was set to 20.0 μm/s. The local raster-scan took 0.785 s while the raster-scan took 16.2 s (~21 times longer).

Integral-Derivative (PID) controller was designed based on the semi-automatic tuning method[22] and the actuators were operated in closed-loop mode. (Note that this tuning method was developed for high-speed AFM and illustrates the ability to combine the local raster-scan algorithm with other high-speed methods.) The Bode plots for the controller and the closed-loop system are also shown in Fig. 3. To simulate sensor noise in the lateral positioning, samples from a zero mean, 1 nm variance Gaussian white noise process were added to the measurements of the x and y piezo positions. Note that while no cross-coupling between the axes was modeled, such effects could easily be included but would require a more complicated controller. As this work focuses on the higher level control algorithm, they were neglected for simplicity.

The cantilever dynamics were modeled as a second-order system while the tip-sample interaction was described using the Derjaguin-Muller-Toporov model.[23] The simulated AFM could be operated in either contact or intermittent-contact (tapping) mode. In this work, tapping mode was used with a nominal amplitude of the cantilever oscillation of 70 nm. The measured amplitude signal was produced by demodulating the cantilever signal and corrupting it by two additive zero mean Gaussian white noise sources. The first, capturing thermal noise, had a standard deviation of 0.1 nm while the second, capturing measurement noise, had a standard

deviation of 0.8 nm. The z controller acted to maintain a set amplitude.

To implement the local raster-scan algorithm, one must choose a detection algorithm for the detector block. In this work, the transient signal detector[16] was selected. This technique detects abrupt changes in the cantilever dynamics and is well-suited for a fast-moving tip. A small, artificial shift between the detected crossing position and the reported value of r_k was added so that the algorithm would estimate the center of the sample rather than the edge.

We simulated two samples placed in a 800 nm by 800 nm area. Each sample had the same cross section of a semi-on top of a block (see Fig. 4). In order to roughly mimic biopolymers, the width was set to 8 nm and the height to 6 nm. One sample path was modeled as a sinusoid along a diagonal line (see Fig. 5(d)) while the path of the other was modeled as a "flower" pattern by periodically varying the radius of a 300 nm circle (see Fig. 6(d)).

For each sample, a standard raster-scan image was made using a line rate of 12.5 Hz and an image resolution of 200 by 200 pixels, corresponding to an average tip speed of 20 μm/s and an imaging time of 16.2 s. A local raster-scan was then made of the same sample using the same tip speed. For each scan, the amplitude parameter was set to $A = 24$ nm and the resolution parameter to $\omega = 1/8$ rad/nm, corresponding to a
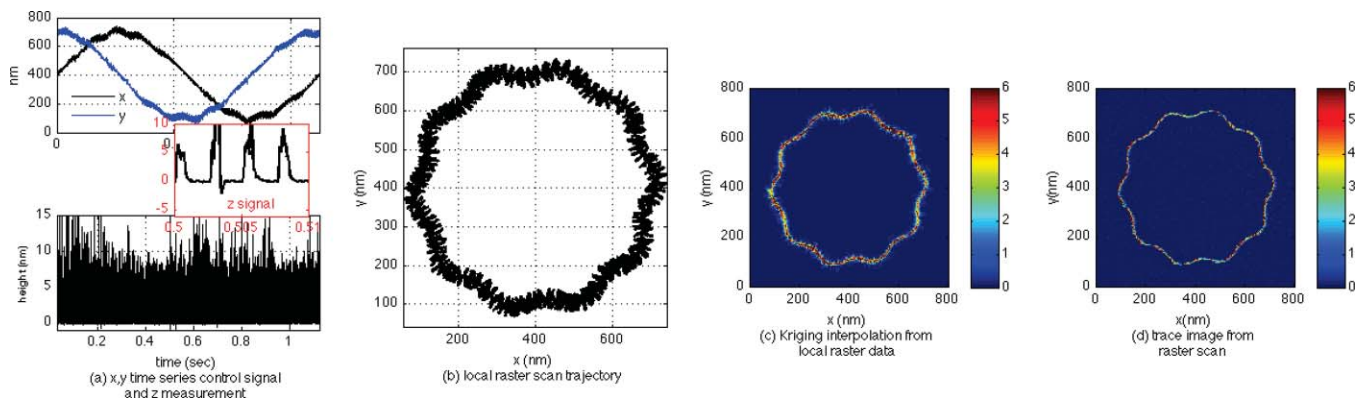

FIG. 6. (Color online) Simulation result of local raster ((a)–(c)) and raster-scan (d) on a flower test curve. Image (b) clearly indicates that the local raster-scan kept the tip in the vicinity of the sample. The tip speed in both images was set to 20.0 μm/s. The local raster-scan took 1.25 s while the raster-scan took 16.2 s (~13 times longer).

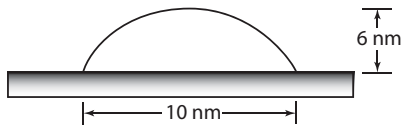FIG. 7. Sample profile used to generate height measurements to drive the local raster-scan algorithm on the nanopositioning stage.

FIG. 8. Bode plot of the close loop response for the two axis of our nanopositioning stage.

nominal spacing between crossings of the sample of 4 nm, making the spatial resolution equivalent to that of the raster-scanned images.

B. Simulation results

The results for the sinusoidal sample are shown in Fig. 5. The data measured along the local raster-scan trajectory are shown in Fig 5(a) and the corresponding trajectory in Fig. 5(b). The local raster-scan image, generating from the modified Kriging method, is shown in Fig. 5(c). The raster-scan image is shown in Fig. 5(d). Note that the noise in the measurements can be seen on the substrate portion of the raster image, as can a small parachuting effect (due to the dynamics of the controller), in which the peak of the sample appears on the leading edge of the scan direction. The Kriging image is set to have the same pixel resolution as the raster-scan image (200 by 200 pixels). The scan time for the local raster-scan algorithm was 0.785 s or 4.85% of the raster-scan imaging time. This reduction is driven by the fact that the algorithm scans a significantly smaller area, greatly reducing the path length followed by the tip.

The results for the flower sample are shown in Fig. 6, with the measured data along the local raster-scan trajectory in Fig 6(a) and the corresponding trajectory in Fig 6(b). The local raster-scan image, generating from Kriging, is shown in Fig. 6(c) and the raster-scan image is shown in Fig. 6(d). As before, the Kriging image has the same pixel resolution. The scan time for the local raster-scan algorithm was 1.25 s, or 7.72% of the standard raster-scan time.

IV. EXPERIMENTS

To illustrate the scanning algorithm on a physical system, the algorithm was used to move a two-axis nanoposi-

tioning stage. In lieu of an AFM head, artificial height measurements were generated as a function of the measured position of the stage. The same two samples as imaged in the simulation were used in the physical experiments, though the profiles were changed to a half-sinusoid with a spatial period of 20 nm (and thus a width of 10 nm) to loosely capture the effect of tip-broadening (see Fig. 7). As in the simulations, the image area was set to 800 nm by 800 nm.

A. System setup

The local raster-scan algorithm was implemented on a digital signal processor DSP (P25M, Innovative Integrations, Simi Valley, CA) at a 10 kHz sampling rate. It was used to control a two-axis nanopositioner comprised of two single-axis actuators stacked together (Nano-HL piezoactuators with NanoDrive 85 controller, Mad City Labs, Madison, WI). The DSP commands were output over a 16-bit digital-to-analog converter, through a custom built converter box that translated the ±2 V output of the DSP to the 0–10 V input range of the piezo controller. The measured position of the nanopositioner was then input to the DSP using a 16-bit analog-to-digital converter and passed through a digital filter. The
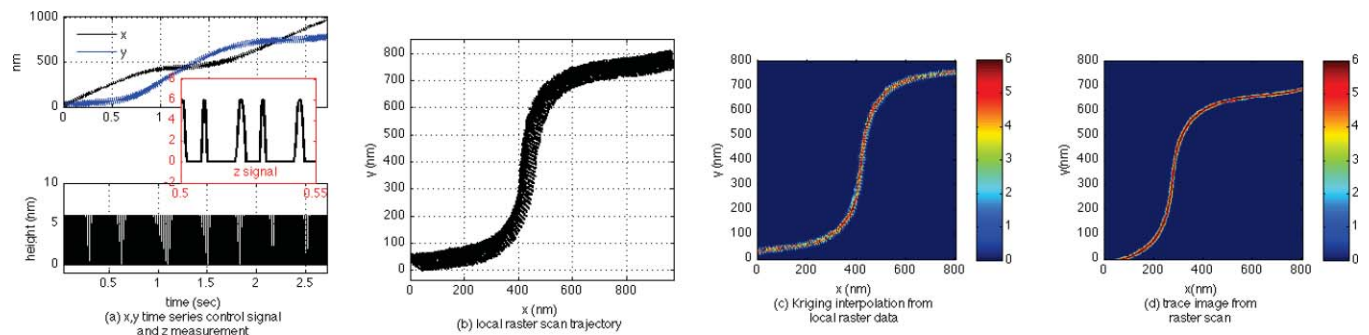

FIG. 9. (Color online) Experimental result of the local raster- ((a)–(c)) and raster-scan (d) on a sinusoidal test curve. As in the simulation results, the algorithm tracked the sample, reducing image time by reducing the image area. The tip speed for both scans was set to 6.5 μm/s. The local raster-scan took 2.57 s while the raster-scan took 49.2 s.
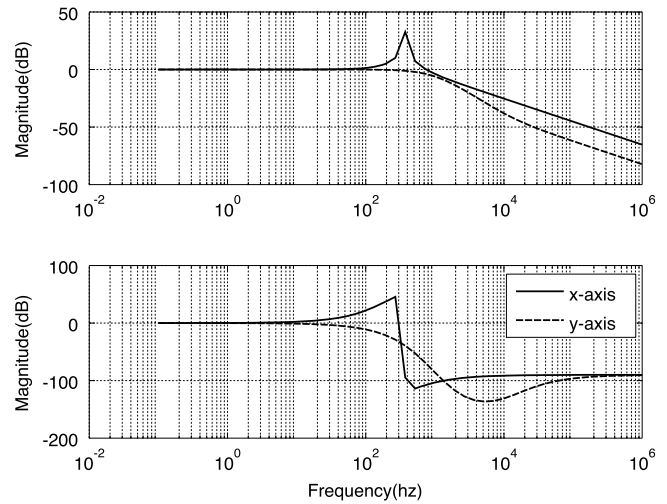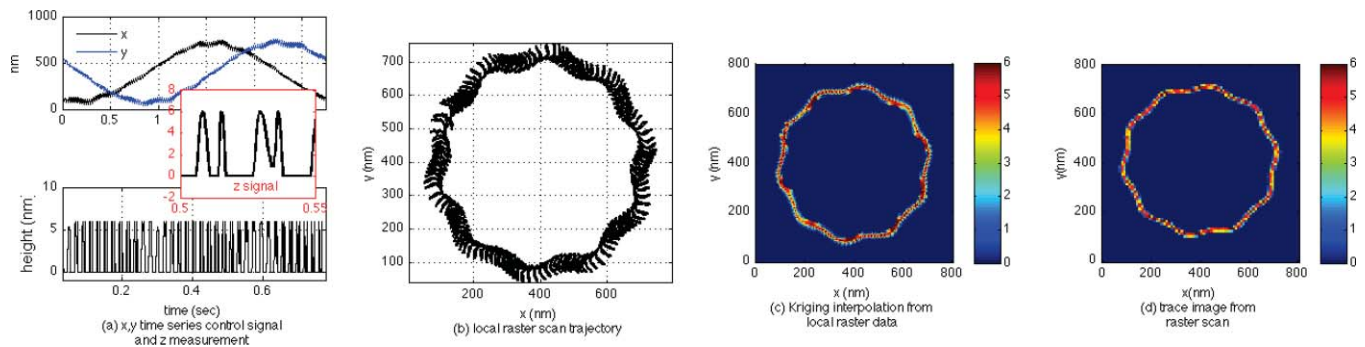
FIG. 10. (Color online) Experimental result of the local raster- ((a)–(c)) and raster-scan (d) on a flower test curve. As in the simulation results, the algorithm tracked the sample, reducing image time by reducing the image area. The tip speed for both scans was set to 6.5 μm/s. The local raster-scan took 2.75 s while the raster-scan took 19.7 s.

closed-loop noise in the system was ∼2 nm in standard deviation. The nanopositioner controller included a manufacturer-designed PI controller for low-level positioning. The Bode plot of the stage dynamics in the two directions is shown in Fig. 8.

Since there was no cantilever dynamics in these experiments, the transient signal detection algorithm could not be used. In its place, a simple threshold algorithm was utilized to determine whether the measurements were on or off the sample. A transition from off to on or on to off triggered an update of the algorithm. After each detection, subsequent detections were delayed for a short period of time to ensure the next detection occurred on the same side of the sample.

In order to allow for real-time execution, the inversion of Eq. (3) to convert time to arclength was performed using a look-up table. In the implementation described here, all calculations for a single step of the algorithm (including sampling, detection, estimation, filtering, $t - s$ conversion, Frenet-Serret frame evolution, tip trajectory calculation, and command output) took ∼30 μs.

The tip speed was set to 6.5 μm/s. Raster-scans were performed over a 1 μm by 1 μm area to eliminate dynamic effects at the edges of the image due to the triangular scan pattern. For the local raster-scan runs, the amplitude parameter was set to $A = 40$ nm. For the sinusoidal sample, the resolution parameter was set to $\omega = 0.2$ rad/nm, corresponding to a nominal spacing of 5 nm between crossings of the sample. For a comparison, the pixel size in the raster-scan was set to 2.5 nm, leading to 200 by 200 pixels in the center 800 nm by 800 nm area. The imaging time for the raster-scan of this region was 49.2 s. For the flower sample, the resolution parameter was set to $\omega = 0.1$ rad/nm, corresponding to 5 nm per sample. The pixel size in the raster-scan was thus also set to 5 nm, leading to 160 by 160 pixels in the center region. The imaging time for the raster-scan of this region was 19.7 s.

B. Results

The results for the sinusoidal sample are shown in Fig. 9. The data measured during the local raster-scan are shown in Fig. 9(a), the trajectory of the tip during the scan in Fig. 9(b), and the corresponding image generated from the data in

Fig. 9(c). The raster-scan image is shown in Fig. 9(d). The scan time for the local raster algorithm was 2.57 s, or 5.2% of the raster-scan time (for just the center 800 nm by 800 nm area).

The results for the flower sample are shown in Fig. 10. The data measured during the local raster-scan are shown in Fig. 10(a), the trajectory of the tip during scan in Fig. 10(b), and the corresponding image generated from the data in Fig. 10(c). The raster-scan image is shown in Fig. 10(d). The scan time for the local raster-scan algorithm was 2.75 s, or 13.94 % of the raster-scan time.

V. SUMMARY

Non-raster methods such as the local raster-scan algorithm presented here are a new and novel way for greatly reducing imaging time in AFM. Improvements by an order-of-magnitude or more will greatly extend the applicability of AFM for studying dynamics in systems with nanometer-scale features.

[1] G. Binnig, C. F. Quate, and C. Gerber, Phys. Rev. Lett. **56**, 930 (1986).
[2] G. Schitter and M. J. Rost, Mater. Today **11**, 40 (2008).
[3] M. B. Viani, T. E. Schäffer, G. T. Paloczi, L. I. Pietrasanta, B. L. Smith, J. B. Thompson, M. Richter, M. Rief, H. E. Gaub, K. W. Plaxco, A. N. Cleland, H. G. Hansma, and P. K. Hansma, Rev. Sci. Instrum. **70**, 4300 (1999).
[4] A. Humphris, M. Miles, and J. Hobbs, Appl. Phys. Lett. **86**, 034106 (2005).
[5] T. Ando, T. Uchihashi, and T. Fukuma, Prog. Surf. Sci. **83**, 337 (2008).
[6] K. K. Leang and A. J. Fleming, Asian J. Control **11**, 144 (2009).
[7] J. A. Butterworth, L. Y. Pao, and D. Y. Abramovitch, in *Proceedings of the American Control Conference, Baltimore, Maryland, 2010* (IEEE, New York, 2010), pp. 5738–5744.
[8] Y. Yan, Q. Zou, and Z. Lin, Nanotechnology **20**, 175301 (2009).
[9] Y. Wu and Q. Zou, IEEE Trans. Control Syst. Technol. **15**, 936 (2007).
[10] G. Schitter, K. Astrom, B. DeMartini, P. Thurner, K. Turner, and P. Hansma, IEEE Trans. Control Syst. Technol. **15**, 906 (2007).
[11] T. Ando, T. Uchihashi, N. Kodera, D. Yamamoto, and A. Miyagi, Eur. J. Physiol. **456**, 211 (2008).

[12] P. Huang and S. B. Andersson, in *Proceedings of the American Control Conference, San Francisco, California, 2011* (IEEE, New York, to be published).

[13] S. B. Andersson, IEEE Trans. Nanobiosci. **6**, 354 (2007).

[14] P. I. Chang and S. B. Andersson, in *Proceedings of the American Control Conference, Seattle, WA, 2008* (IEEE, New York, 2008), pp. 3207–3212.

[15] P. I. Chang and S. B. Andersson, in *Proceedings of the IEEE Conference on Decision and Control, Shanghai, China, 2009* (IEEE, New York, 2009), pp. 8290–8295.

[16] D. R. Sahoo, A. Sebastian, and M. V. Salapaka, Appl. Phys. Lett. **83**, 5521 (2003).

[17] P. I. Chang and S. B. Andersson, in *Proceedings of the American Control Conference, St. Louis, Missouri, 2009* (IEEE, New York, 2009), pp. 2266–2271.

[18] M. Rubenstein and R. Colby, *Polymer Physics* (Oxford University Press, New York, 2003).

[19] E. H. Isaaks and R. M. Srivastava, *Applied Geostatistics* (Oxford University Press, New York, 1989).

[20] D. Lee and B. Schachter, Int. J. Comput. Inf. Sci. **9**, 219 (1980).

[21] D. Y. Abramovitch, S. B. Andersson, L. Y. Pao, and G. Schitter, in *Proceedings of the American Control Conference, New York, 2007* (IEEE, New York, 2007), pp. 3488–3502.

[22] D. Y. Abramovitch, S. Hoen, and R. Workman, in *Proceedings of the American Control Conference, Seattle, Washington, 2008* (IEEE, New York, 2008), pp. 2684–2689.

[23] A. Sebastian, M. V. Salapaka, D. J. Chen, and J. P. Cleveland, J. Appl. Phys. **89**, 6473 (2001).